

Dilution and microsegregation in dissimilar metal welds between super austenitic stainless steel and nickel base alloys

S. W. Banovic, J. N. DuPont, and A. R. Marder

Super austenitic stainless steels are often welded using high Mo, Ni base filler metals to maintain the corrosion resistance of the weld. An important aspect of this processing is the weld metal dilution level, which will control the composition and resultant corrosion resistance of the weld. In addition, the distribution of alloying elements within the weld will also significantly affect the corrosion resistance. Dissimilar metal welds between a super austenitic stainless steel (AL-6XN) and two Ni base alloys (IN625 and IN622) were characterised with respect to their dilution levels and microsegregation patterns. Single pass welds were produced over the entire dilution range using the gas tungsten arc welding process. Microstructural characterisation of the welds was conducted using light optical microscopy, scanning electron microscopy, and quantitative image analysis. Bulk and local chemical compositions were obtained through electron probe microanalysis. The quantitative chemical information was used to determine the partition coefficients k of the elements in each dissimilar weld. The dilution level was found to decrease as the ratio of volumetric filler metal feedrate to net arc power increased. Reasons for this behaviour are discussed in terms of the distribution of power required to melt the filler metal and base metal. In addition, the segregation potential of Mo and Nb was observed to increase (i.e. their k values decreased) as the Fe content of the weld increased. This effect is attributed to the decreased solubility of Mo and Nb in austenite with increasing Fe additions. Since the Fe content of the weld is controlled by dilution, which in turn is controlled by the welding parameters, the welding parameters have an indirect influence on the segregation potential of Mo and Nb. The results of the present work provide practical insight for corrosion control of welds in super austenitic stainless steels.

STWJ1306

The authors are in the Department of Materials Science and Engineering, Lehigh University, 5 East Acker Avenue, Bethlehem, PA 18015, USA (jnd1@lehigh.edu). Manuscript received 4 June 2001; accepted 11 April 2002.

© 2002 IoM Communications Ltd. Published by Maney for the Institute of Materials, Minerals and Mining.

INTRODUCTION

Increasing importance is being placed upon using a filler metal having a composition significantly different from that of the substrate during fusion welding in order to compensate for diminished mechanical or electrochemical properties. This technique is commonly used during welding

of super austenitic stainless steels. These relatively high Ni stainless steels contain Mo additions (~5–7 wt-%) for improved corrosion resistance. However, during solidification of the weld, Mo segregates preferentially to the liquid, owing to the low solubility of Mo in the austenite phase (γ), and leaves the first solid to form depleted in Mo.¹ In addition, the low diffusion rate of Mo in γ does not allow for Mo to diffuse back towards the dendrite cores to eliminate the concentration gradient.² This can lead to poor corrosion resistance of the weld metal. Previous research has shown that the depleted dendrite cores are susceptible to preferential corrosion due to the low, localised Mo concentrations.^{3–6} To compensate for this effect, high Mo, Ni base filler metals such as IN625 (~9 wt-%Mo) and IN622 (~14 wt-%Mo) are often utilised during fusion welding of such alloys. Although these filler metals do not eliminate microsegregation of Mo, the dendrite core Mo contents in the fusion weld are increased relative to those in autogenous welds, and this helps to minimise preferential attack at the dendrite cores.

With this approach, the final distribution of Mo (and other alloying elements) will be controlled by the filler metal composition, welding parameters (which control the nominal weld metal composition), and the segregation potential of each element. In addition, interactive effects may exist in which the segregation potential of an alloying element depends on the nominal weld composition. Therefore, as potentially wide ranges of weld metal composition and microsegregation behaviour are possible in practice, a large variation in corrosion resistance may be encountered. However, no detailed study has been reported which investigates the relationship between welding parameters, nominal weld composition, and resultant microstructure in detail to address these potential problems. Thus, the objective of the present research was to characterise the microstructures of fusion welds in a common super austenitic stainless steel (AL-6XN) as a function of filler metal composition (using IN625 and IN622) and welding parameters. The results of the present work will be useful for ultimately controlling the corrosion resistance of welds in this alloy.

EXPERIMENTAL PROCEDURE

Dissimilar bead on plate welds were produced between AL-6XN and IN625 or IN622 using the gas tungsten arc welding (GTAW) process by directly feeding the filler metal into the weld pool of the substrate. The travel speed was fixed at 2.0 mm s⁻¹ with a 2.5 mm arc gap. The average voltage was 13.9 V ± 1.3 V. The AL-6XN and IN625 were obtained in both plate and wire form, whereas IN622 wire and C-22 plate (compositional equivalent for IN622) were used for the other Ni base alloy. Their respective compositions are given in Table 1. The full range of weld metal compositions that could exist between AL-6XN and IN622 or IN625 were produced by systematic variations in

Table 1 Compositions of raw materials as determined using electron probe microanalysis (EPMA): all values are in wt-% (values in parentheses represent standard deviations)

Material	Form	Fe	Ni	Cr	Mo	Nb	Mn	Si	Other
AL–6XN	Wire	47.6 (0.7)	23.9 (0.5)	21.3 (1.1)	6.1 (0.4)	0.0 (0.0)	0.2 (0.1)	0.3 (0.1)	0.8 ...
	Plate	47.0 (0.8)	24.4 (0.3)	20.9 (1.0)	6.3 (0.3)	0.0 (0.0)	0.2 (0.0)	0.3 (0.1)	0.9 ...
IN625	Wire	0.6 (0.2)	64.6 (1.2)	21.7 (1.7)	8.9 (0.5)	3.5 (0.6)	0.0 (0.0)	0.1 (0.0)	0.6 ...
	Plate	4.5 (0.3)	60.8 (0.9)	20.8 (1.1)	8.7 (0.7)	3.5 (0.4)	0.1 (0.0)	0.2 (0.0)	1.4 ...
IN622	Wire	2.4 (0.1)	59.0 (1.8)	20.5 (0.7)	14.3 (0.6)	0.0 (0.0)	0.2 (0.0)	0.0 (0.0)	3.4 ...
C–22	Plate	3.6 (0.2)	56.7 (1.5)	21.3 (1.1)	13.2 (0.5)	0.0 (0.0)	0.2 (0.0)	0.0 (0.0)	5.0 ...

filler metal feed speed and arc current (Table 2). To achieve this full range, welds were first produced on the AL–6XN base metal using both IN622 and IN625 filler metals. This provided welds that consisted of from 100% to as little as 30% of the AL–6XN base metal. The remaining weld metal compositions were produced by using either IN625 or C–22 plates as the base metal and AL–6XN as the filler metal. The level of mixing between the substrate and filler metal was quantified through measurement of the weld metal dilution level. These levels were determined via two methods: chemical analysis and geometric dilution measurements. For the former, dilution was determined using electron probe microanalysis (EPMA). As explained below, the electron probe was rastered over of an area of approximately 1500 μm² for these measurements to obtain an average weld metal composition and thereby to average out effects from microsegregation. In the fully mixed fusion zone, the final weld composition will simply be a mixture of the base metal and filler metal compositions as follows

$$C_{fz} = C_{fm}(1 - D) + C_s(D) \quad \dots \quad (1)$$

where C_{fz} , C_{fm} , and C_s are the elemental compositions of the fusion zone, filler metal, and substrate, respectively, and D is the dilution level. Thus, when C_{fz} , C_{fm} , and C_s are all known, the dilution level, expressed as a fraction, is simply determined by

$$D = (C_{fz} - C_{fm}) / (C_s - C_{fm}) \quad \dots \quad (2)$$

The values for the major constituents, namely, Fe and Ni

were used and averaged to obtain the final dilution level of the weld. Dilution levels were also determined using metallographic methods to measure the individual geometric cross-sectional areas of the deposited filler metal and melted substrate. The ratio of the melted substrate area A_s to the total melted cross-sectional area from the filler metal A_{fm} and substrate A_s is the dilution level, again expressed as a fraction as follows

$$D = A_s / (A_s + A_{fm}) \quad \dots \quad (3)$$

Dilution levels are given in Table 2 as calculated values using equation (3). In addition, values of $1 - D$ are provided for the Ni base alloys. These values are reported because they provide the dilution level with respect to AL–6XN. These values will allow the dilution levels to be more conveniently reported with a range of 0.0 to 1.0, where 0.0 and 1.0 represent autogenous welds on the Ni base and AL–6XN alloys, respectively. Only dilution levels calculated for the alloys with Ni base substrates will be reported differently as their values calculated from equation (3) were subtracted from 1.0. Unless otherwise stated, the dilution levels will be reported as percentages, multiplying D by 100%, and with respect to AL–6XN as the base material.

Samples were removed from the welds using an abrasive cutoff wheel, mounted in cold setting epoxy, and polished to a 0.04 μm finish using colloidal silica. Samples having stainless steel substrates were electrolytically etched in a mixture of nitric acid (HNO₃) and water (H₂O) in the proportions of 60/40. The voltage was preset at 5 V and pure

Table 2 Processing parameters used to fabricate single pass, dissimilar metal welds, and resulting geometric dilution levels

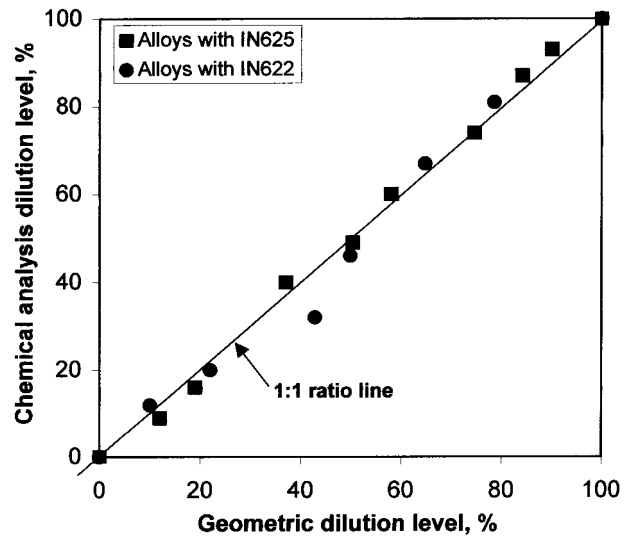
Sample	Base metal	Filler metal	Arc current, A	Volumetric filler metal feedrate, mm ³ s ⁻¹	Geometric dilution level (as determined from equation (3)), × 100%	Dilution level (with respect to AL–6XN as base metal), (1.00 – D) × 100%
1	AL–6XN	...	150	0	100	...
2	AL–6XN	IN625	250	5.9	90	...
3	AL–6XN	IN625	250	11.7	84	...
4	AL–6XN	IN625	300	35.1	75	...
5	AL–6XN	IN625	325	58.7	58	...
6	AL–6XN	IN625	275	46.9	50	...
7	IN625	AL–6XN	250	39.0	63	37
8	IN625	AL–6XN	250	19.5	81	19
9	IN625	AL–6XN	300	19.5	88	12
10	IN625	...	150	0	100	0
11	AL–6XN	IN622	250	12.4	78	...
12	AL–6XN	IN622	300	37.2	65	...
13	AL–6XN	IN622	275	49.7	50	...
14	AL–6XN	IN622	325	74.5	43	...
15	C–22	AL–6XN	300	29.2	78	22
16	C–22	AL–6XN	300	19.5	90	10
17	C–22	...	150	0	100	0

platinum was used as the cathode. A 10% oxalic acid solution was used for etching samples having Ni base substrates under the same conditions. Microstructural characterisation was performed using light optical microscopy (LOM) and scanning electron microscopy (SEM). Quantitative bulk and local chemical analysis was carried out using EPMA. A Jeol 733 SuperProbe, equipped with wavelength dispersive spectrometers, was operated at an accelerating voltage and probe current of 15 kV and 20 nA, respectively. Bulk results were obtained from areas of approximately 1500 μm^2 , sufficiently large to avoid any deviations due to microsegregation. Localised microsegregation measurements were also obtained by holding the electron beam stationary. In the analysis of Fe, Ni, and Cr, K_{α} X-ray lines were used, whereas Nb and Mo required L_{α} X-ray lines for analysis. Other elements present in minimal quantities were not analysed. These counts were converted to weight percentages using a ZAF correction scheme.⁷ The volume fraction of the second phase present in the interdendritic regions of the welds was measured using a Leco 3001 quantitative image analysis system.

Differential thermal analysis (DTA) was conducted on selected samples that were carefully sectioned out of the homogenous portion of the fusion zone of the dissimilar metal welds, as described below. Samples were heated to 10 K above their liquidus temperatures at 5 K min^{-1} and cooled at 20 K min^{-1} to room temperature. This procedure

Table 3 Compositions (wt-%) for experimental alloys with IN625 and IN622 filler metals as determined using EPMA: values in parentheses represent standard deviations

Dilution level	Fe	Ni	Cr	Mo	Nb	Mn	Si	Other
IN625 filler								
100%	46.9 (0.6)	23.5 (0.4)	21.6 (0.7)	6.2 (0.4)	0.0 (0.0)	0.3 (0.0)	0.3 (0.1)	1.2 ...
90%	41.9 (0.5)	25.2 (0.3)	21.5 (0.5)	6.7 (0.4)	0.2 (0.1)	0.4 (0.0)	0.3 (0.0)	3.8 ...
84%	39.3 (0.6)	28.4 (0.3)	21.4 (0.3)	6.4 (0.5)	0.5 (0.2)	0.4 (0.0)	0.2 (0.0)	3.3 ...
75%	33.8 (0.3)	33.6 (0.8)	21.1 (0.2)	6.8 (0.2)	1.1 (0.5)	0.4 (0.0)	0.1 (0.0)	3.2 ...
58%	26.4 (0.7)	38.6 (0.5)	21.0 (0.4)	7.6 (0.4)	1.5 (0.4)	0.3 (0.1)	0.2 (0.0)	4.4 ...
50%	22.1 (0.9)	43.7 (0.2)	21.0 (0.5)	7.7 (0.3)	2.0 (0.4)	0.3 (0.0)	0.1 (0.0)	3.1 ...
37%	20.2 (0.1)	45.2 (0.7)	21.0 (0.2)	7.7 (0.1)	2.2 (0.3)	0.4 (0.0)	0.2 (0.0)	3.2 ...
19%	10.6 (0.2)	54.5 (0.5)	20.0 (0.4)	8.2 (0.2)	2.9 (0.4)	0.3 (0.0)	0.1 (0.0)	3.4 ...
12%	7.7 (0.1)	57.0 (0.4)	20.5 (0.4)	8.4 (0.3)	3.3 (0.8)	0.3 (0.0)	0.2 (0.0)	2.5 ...
0%	4.6 (0.3)	61.4 (1.2)	20.4 (0.6)	8.5 (0.4)	3.5 (0.1)	0.2 (0.0)	0.1 (0.0)	1.3 ...
IN622 filler								
100%	46.9 (0.6)	23.5 (0.4)	21.6 (0.7)	6.2 (0.4)	0.0 (0.0)	0.3 (0.0)	0.3 (0.1)	1.2 ...
78%	37.2 (0.4)	30.0 (0.2)	21.8 (0.4)	7.1 (0.5)	0.0 (0.0)	0.3 (0.0)	0.3 (0.0)	3.3 ...
65%	30.4 (0.6)	34.5 (0.7)	21.5 (0.5)	8.1 (0.2)	0.0 (0.0)	0.3 (0.0)	0.2 (0.1)	5.0 ...
50%	21.5 (0.6)	42 (1.1)	22.1 (0.5)	9.9 (0.3)	0.0 (0.0)	0.3 (0.0)	0.2 (0.1)	4.0 ...
43%	14.7 (1.0)	46.3 (1.1)	21.7 (0.8)	10.2 (0.4)	0.0 (0.0)	0.3 (0.1)	0.1 (0.1)	6.7 ...
22%	12.3 (0.6)	50.1 (1.5)	23.0 (0.8)	11.6 (0.5)	0.0 (0.0)	0.4 (0.0)	0.1 (0.0)	2.5 ...
10%	8.6 (0.4)	52.7 (1.2)	22.4 (0.9)	12.4 (0.8)	0.0 (0.0)	0.4 (0.0)	0.1 (0.0)	3.5 ...
0%	3.8 (0.3)	57.9 (1.1)	22.3 (1.3)	13.1 (0.4)	0.0 (0.0)	0.4 (0.0)	0.1 (0.0)	2.5 ...



1 Comparison of dilution levels as determined using both chemical analysis and geometric calculations

was conducted under flowing argon to avoid oxidation of the sample. These samples were also microstructurally characterised using the techniques described above.

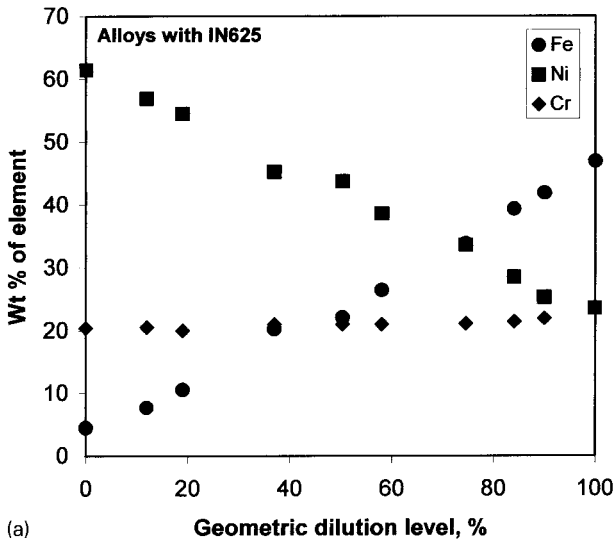
RESULTS AND DISCUSSION

Dilution levels

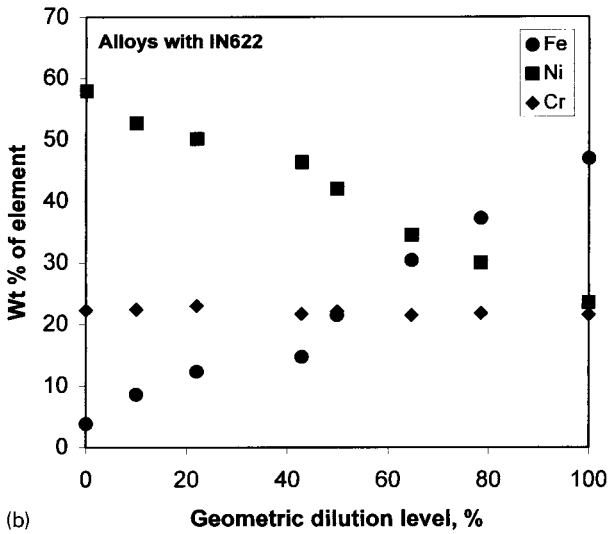
Bulk quantitative chemical information was obtained for the fusion zone of the welds using EPMA, and these data are presented in Table 3. The dilution levels as determined from both chemical analysis and geometrical measurements are compared in Fig. 1. Good agreement can be seen between the two types of measurement. Unless otherwise indicated, all dilution values discussed will be the geometric dilution values. In addition, as described previously, the D values for the Ni base alloys will be reported with respect to AL–6XN by using the $1 - D$ values. (It should be noted that the Mn levels presented in Table 3 exhibit a systematic error. The Mn levels in the filler metals and substrates are between 0 and 0.2 wt-%. Thus, the fusion zone values should always lie within this range or possibly be lower owing to evaporation. However, the EPMA data given in Table 3 consistently show higher values. This error is attributed to the detection limits of the EPMA, in which errors in detection of elements present in small quantities are common.)

Figure 2 shows the composition variation for the major matrix elements (Fe, Ni, Cr) as a function of the geometrical dilution levels. A similar plot for the minor elements Mo and Nb (the latter for alloys with IN625 only) can be seen in Fig. 3. Figure 2 shows that as the dilution levels increase, the amounts of Fe and Ni change inversely to each other whereas the amount of Cr remains approximately constant. Such trends would be expected as more of the Fe rich substrate is mixed with the Ni base filler metal as the dilution level increases. There is a slight deviation in linearity for the Fe concentration values in Fig. 2 because the Fe concentration of the filler metal is slightly different from that of the substrate. In Fig. 3, the increase in dilution leads to lower Mo and Nb concentrations in the weld metal.

The dilution level controls both the nominal weld metal composition and, as will be discussed in more detail below, the segregation potential of alloying elements in the weld. Thus, careful control over dilution is required to control the resultant corrosion resistance of the weld. It has previously been demonstrated that the dilution is highly sensitive to the welding parameters and will depend primarily on the



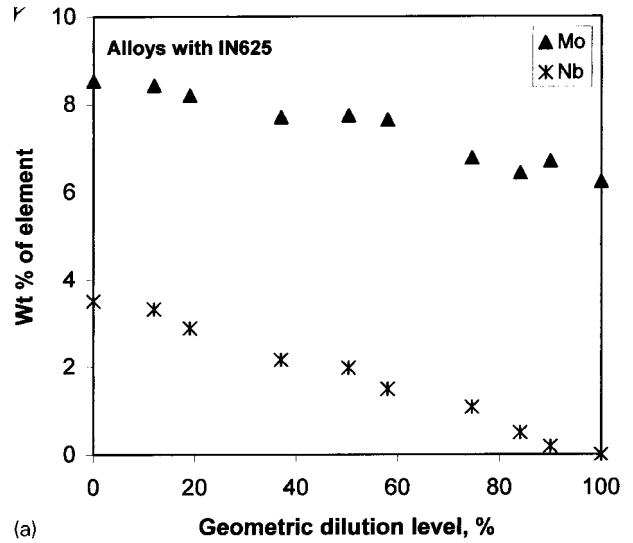
(a)



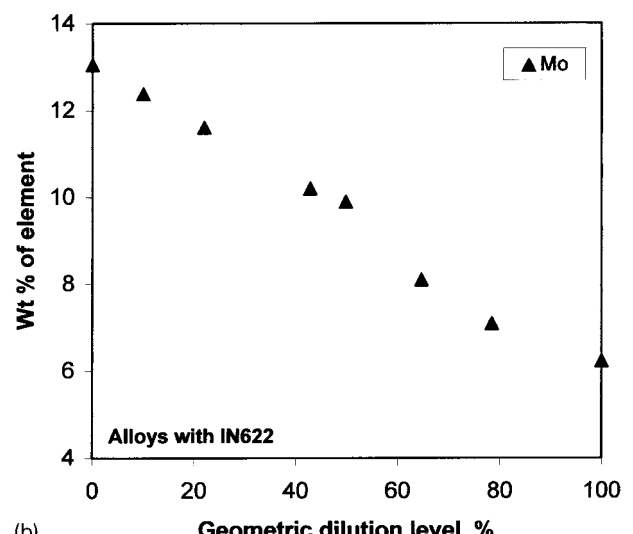
(b)

2 Bulk chemical information for major matrix elements plotted as function of geometric dilution level for *a* alloys with IN625 and *b* alloys with IN622

volumetric filler metal feedrate and arc power.⁸ This is shown in Fig. 4, where the geometric dilution level is correlated with the ratio of the volumetric filler metal feedrate V_{fm} to the net arc power $\eta_a P$, where η_a is the arc efficiency (0.67 for the GTAW process⁸). For this plot only, the actual dilution levels calculated from equation (3) were used for alloys prepared with AL-6XN filler metal. The dilution is controlled by the relative melting rates of the filler metal and base metal, which in turn are determined by the distribution of arc power between the base metal and filler metal. For example, as the filler metal feedrate is increased for a fixed arc power, the fraction of the arc power used to melt the filler metal increases, and less power remains for melting the substrate. Thus, the dilution level decreases as less substrate melts and mixes with the filler metal. Conversely, if the filler metal feedrate is decreased for a fixed arc power, then the fraction of arc power required to melt the filler metal decreases, and the fraction of power remaining to melt the base metal increases. Under this condition, a larger amount of base metal melts and the dilution level increases. These details (which have been quantified through process modelling in Ref. 8) account for the observed trend shown in Fig. 4. Thus, dilution can be minimised by maximising the volumetric filler metal feedrate to net arc power ratio.

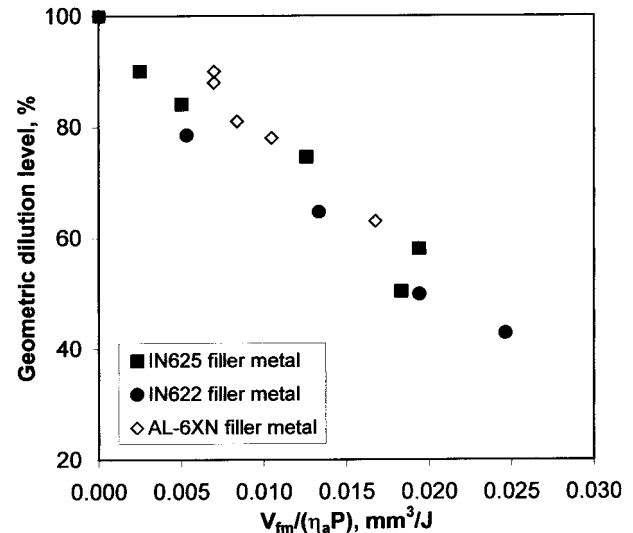


(a)

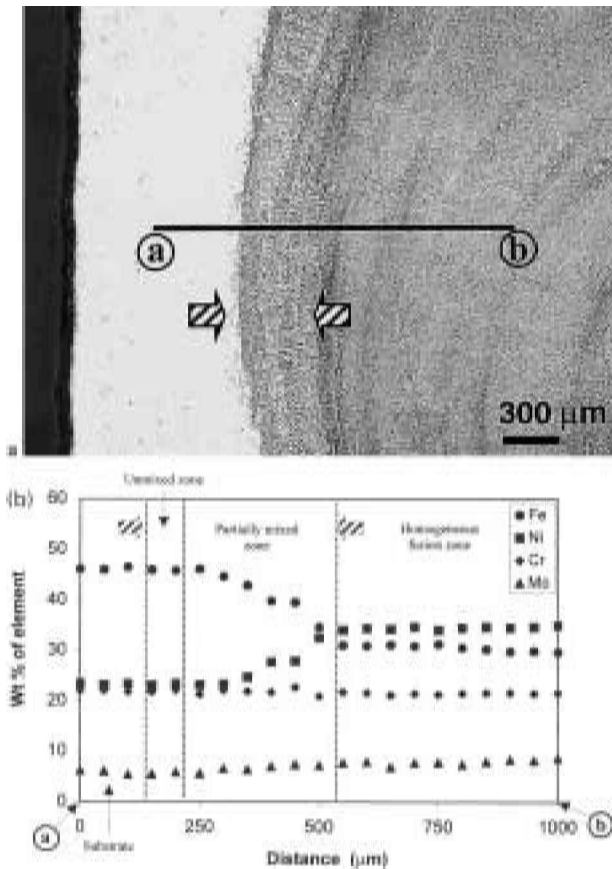


(b)

3 Bulk chemical information for minor elements plotted as function of geometric dilution level for *a* alloys with IN625 and *b* alloys with IN622



4 Geometric dilution level as function of ratio of volumetric filler metal feedrate to net arc power: for welds prepared with AL-6XN filler, actual dilution levels calculated from equation (3) were used

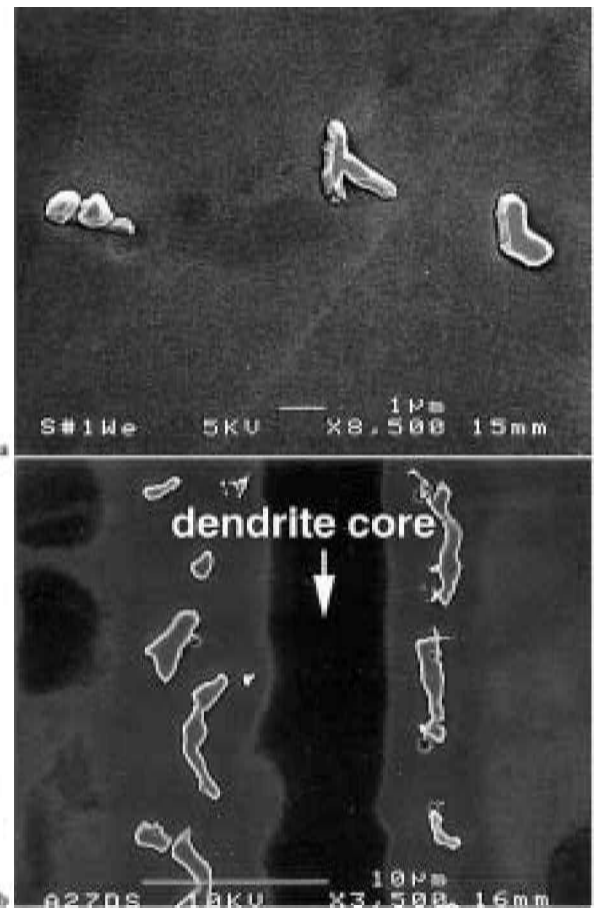


5 *a* light optical micrograph of dissimilar metal weld (65% dilution, with IN622) near fusion line, showing region that etched differently from rest of structure (as indicated by arrows), and *b* electron probe micro-analysis (EPMA) trace through structure shown in *a*, showing various zones found in weld: trace in *b* is not to scale with image in *a*

Weld metal microstructures

Figure 5*a* shows a characteristic microstructure of the dissimilar welds in cross-section, with the welding direction normal to the plane of the paper. This particular image was taken near the fusion line of a weld on AL–6XN prepared with IN622 at a dilution level of 65%. There was a region near the fusion line that etched differently from the rest of the fusion zone (arrowed in Fig. 5*a*). This was observed in all the dissimilar metal weld samples examined and may be explained by a difference in composition or a change of microstructural scale. The EPMA traces (Fig. 5*b*) obtained across these regions showed that this was the combination of the partially mixed zone and the unmixed zone. These two regions are common in dissimilar welds as complete mixing does not occur near the fusion line owing to the presence of a stagnant boundary layer.⁶ In passing from the substrate (*a*’ in Fig. 5) into the homogeneous fusion zone, where good mixing did occur (*b*’ in Fig. 5), a gradual transition in composition can be observed. The extent of the unmixed zone was determined by observing the placement of the microprobe during the trace on the actual microstructure. The size of these two zones generally increased with increasing wire feed speed. Similar results have also been obtained in other alloy systems.⁹

Figure 6 shows SEM images of the typical phases observed in autogenous welds of AL–6XN and welds prepared with the IN622 filler metal. In these welds, an interdendritic phase having a globular morphology was observed. Differential thermal analysis samples from welds



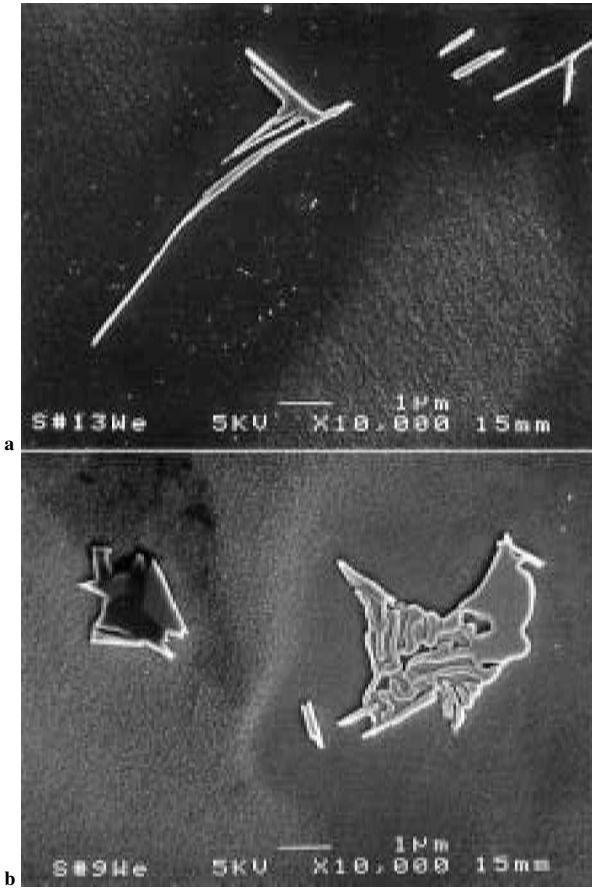
6 Characteristic morphologies of secondary phases observed in interdendritic regions of *a* autogenous weld of AL–6XN and *b* welds prepared with IN622 (SEM)

prepared with IN622 showed identical results. The interdendritic phases in the DTA samples were larger because of the lower cooling rates and could be analysed using EPMA. Typical results are given in Table 4. The composition of this phase is consistent with the sigma (σ) phase commonly observed in welds of AL–6XN.¹⁰ As this phase is commonly found in AL–6XN and in IN622, it is not unexpected to find it in the present set of dissimilar welds.^{10,11} Note that the sigma phase is high in Cr and very high in Mo.

Figure 7 shows SEM images of the typical phase morphologies observed in welds prepared with the IN625 filler. There were two types of phase observed in these welds – one often referred to in the literature as a ‘Chinese script’ morphology (Fig. 7*a*), and one having a eutectic type morphology (Fig. 7*b*).^{12,13} The DTA samples exhibited secondary phases with similar morphologies, but the phases were not sufficiently large to obtain accurate quantitative information using EPMA. Qualitative energy dispersive

Table 4 Compositions (wt-%) for second phases found within interdendritic region of dissimilar metal weld samples after differential thermal analysis: compositions determined via EPMA (values in parentheses represent standard deviations)

Fe	Ni	Cr	Mo	Nb	Mn	Si	Other
31.1	14.9	25.5	25.9	0.0	0.3	0.4	1.9
(1.5)	(0.3)	(1.1)	(2.4)	(0.0)	(0.0)	(0.0)	...



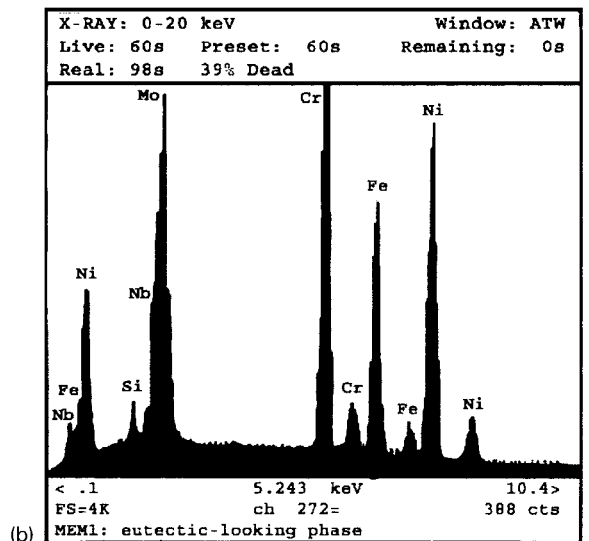
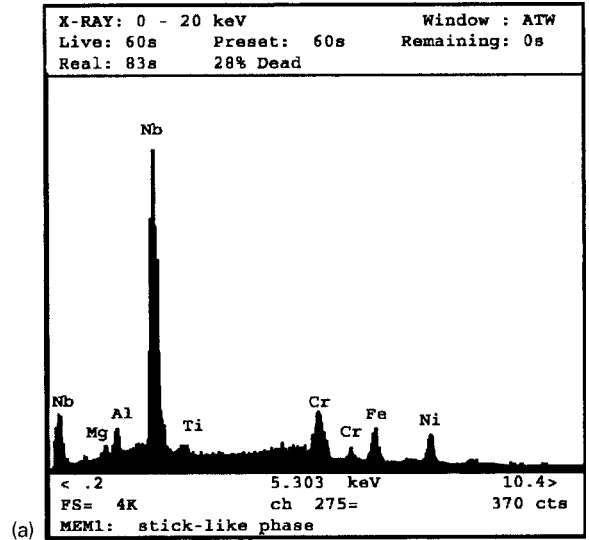
a 'Chinese script' morphology; b eutectic type morphology

spectroscopy (EDS) results collected from the phases exhibiting the Chinese script and eutectic type morphology are shown in Fig. 8a and b, respectively. Note that the Chinese script phase is very high in Nb. It has been well established that Nb bearing superalloys terminate solidification by the formation of a NbC phase having this Chinese script morphology and a γ /Laves constituent that exhibits a eutectic type morphology.^{12,14,15} This is consistent with the SEM images and EDS spectra shown in Figs. 7 and 8. More detailed analysis of these phases will be presented in a future report. Quantitative image analysis was conducted to determine the total amount of secondary phase within the fusion zones. Figure 9 shows that as the geometric dilution level decreased the amount of secondary phase increased for welds prepared with IN625, but remained relatively constant for samples prepared with IN622.

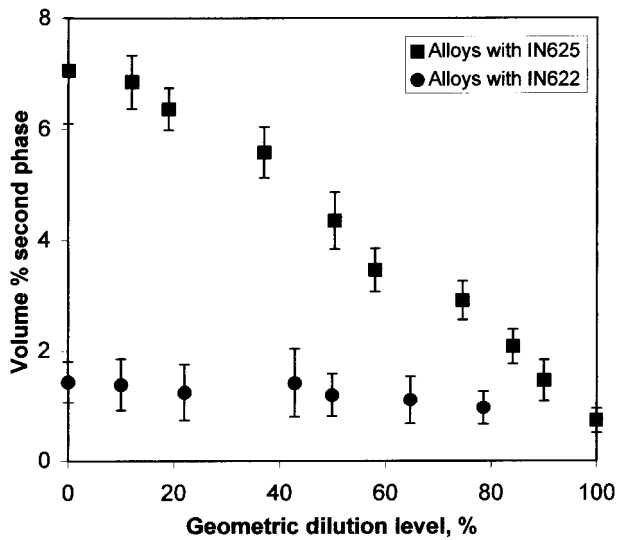
Elemental segregation

To investigate the segregation patterns that occurred upon solidification, EPMA traces were conducted across the dendritic substructures found within the fusion zone of the welds. Figures 10–12 show typical EPMA traces and the corresponding areas that were analysed. For most welds, the dendrite cores were depleted in Mo and Nb (the latter for alloys with IN625 only) and enriched in Fe and Ni. In general, Cr had a slight tendency to segregate to the liquid.

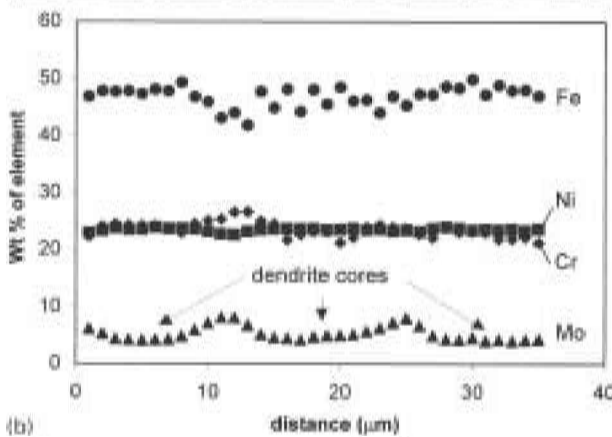
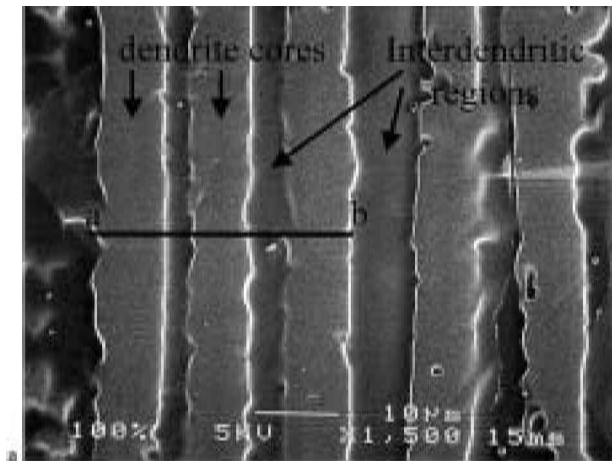
Electron probe microanalysis traces were also conducted across the dendritic substructures in the unmixed zone of the dissimilar metal welds. In these areas of the fusion zone, the presence of the dendritic substructure was a direct



8 Energy dispersive spectra collected from a NbC and b Laves phases in welds prepared with IN625



9 Total amount of secondary phase measured in fusion zone for both sets of dissimilar metal welds, plotted as function of geometric dilution level

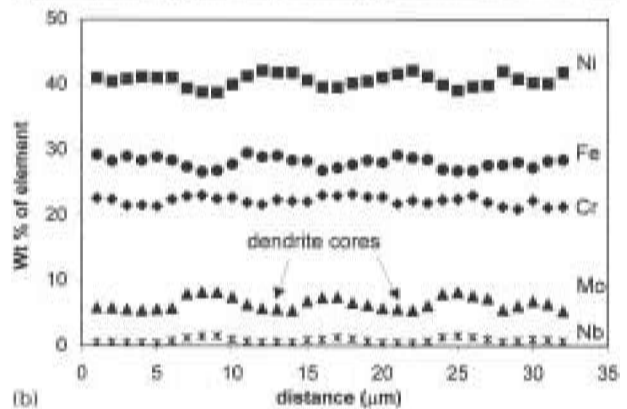
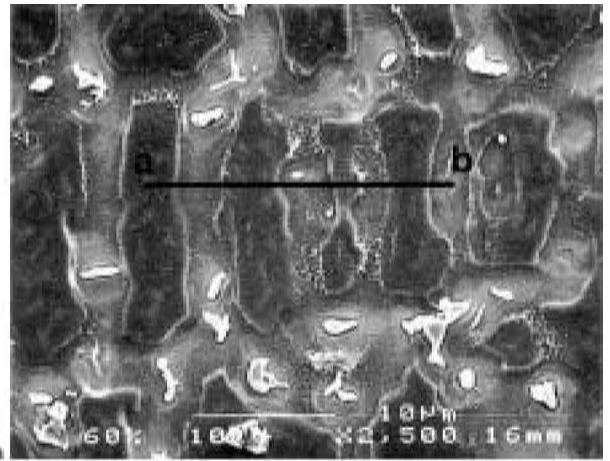


a analysed area (SEM); b microprobe trace

10 Characteristic segregation pattern observed for dendritic substructure of autogenous weld of AL–6XN

indication that melting had occurred, but EPMA traces showed that the nominal Mo content is identical to that of the base metal (Fig. 5b), and thus no mixing with the filler metal occurred. On welds prepared with the AL–6XN base metal, the scans across the unmixed zone showed that the dendrite Mo core concentration was identical to that in the fusion zone of an autogenous weld on AL–6XN, i.e. the scans were similar to that shown in Fig. 10b. This is an important observation which indicates that, regardless of the filler metal composition, an unmixed zone will always exist which contains dendrite core concentrations equivalent to that of an autogenous weld. Thus, it is not possible to increase the core composition of the dendrites in the unmixed zone.

The EPMA data are summarised in Figs. 13 and 14, which show the Mo and Nb nominal and dendrite core compositions for all the welds. For both sets of data, as the dilution level increased, both the nominal and dendrite core compositions of Mo and Nb decreased. Also included in Fig. 13b are the dendrite core compositions from two DTA samples extracted from welds prepared with IN622. These samples were analysed to assess the potential for back diffusion of Mo toward the dendrite cores during the lower cooling rate DTA conditions. It is interesting to note that, although the DTA samples were solidified at a rate of only 20 K min⁻¹ (i.e. a significantly lower cooling rate than for the welds), the Mo core concentrations are essentially equivalent to those in the welds of identical nominal compositions. Thus, the Mo core concentration is essentially independent of cooling rate within the range of cooling rate considered in the present work.



a analysed area (SEM); b microprobe trace

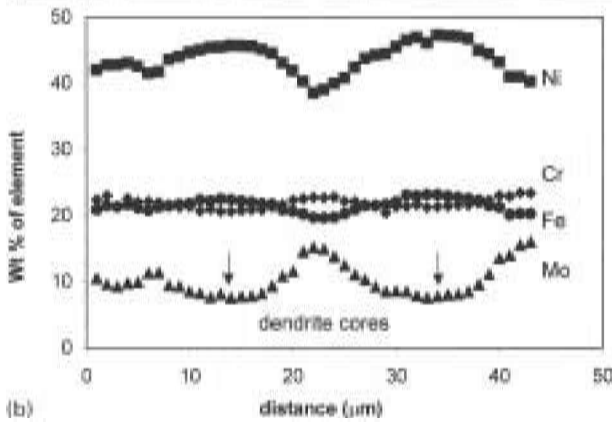
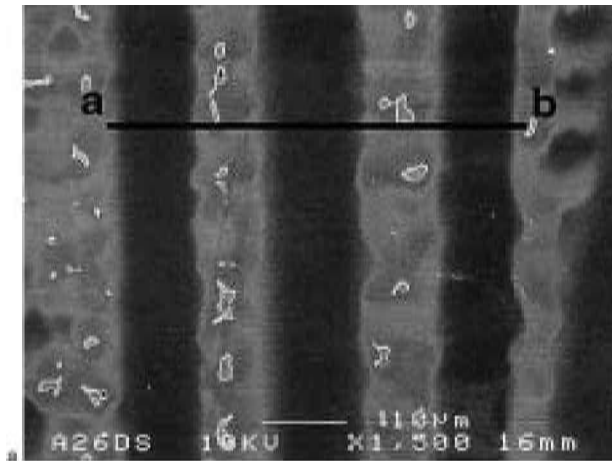
11 Characteristic segregation pattern observed for dendritic substructure of dissimilar metal weld with IN625, 58% dilution level

This cooling rate independence of microsegregation stems from the offsetting effects of increasing solidification time and increasing diffusion distance that occur with decreasing cooling rate. As the cooling rate decreases, there is more time available for back diffusion down the concentration gradient towards the dendrite core. However, the length of the concentration gradient (i.e. the distance over which the solute must diffuse to eliminate the concentration gradient) also becomes larger owing to an increase in cell size with decreasing cooling rate. Thus, these two effects tend to offset each other, and the experimental data suggest that the potential for back diffusion is essentially cooling rate independent under the range of cooling rate investigated in the present work for DTA and arc welding. (It should be noted that, at higher cooling rates typical of high energy density welding processes, dendrite tip undercooling can occur, which enriches the core composition and has the effect of reducing microsegregation. This effect is not considered here.)

Under conditions in which solid state diffusion is negligible, the EPMA data can be used to determine the distribution coefficient *k* of each alloying element via the relationship

$$k = C_{\text{core}}/C_0 \dots \dots \dots (4)$$

where *C*_{core} is the dendrite core composition and *C*₀ is the nominal composition. This provides a measure of *k* at the start of solidification. The *k* values of the major alloying elements for the welds investigated are presented in Tables 5 and 6. These values are important from a corrosion perspective because they dictate the dendrite core composition of the weld. A *k* value near unity indicates that the element



a analysed area (SEM); b microprobe trace

12 Characteristic segregation pattern found for dendritic substructure of dissimilar metal weld with IN622, 43% dilution level

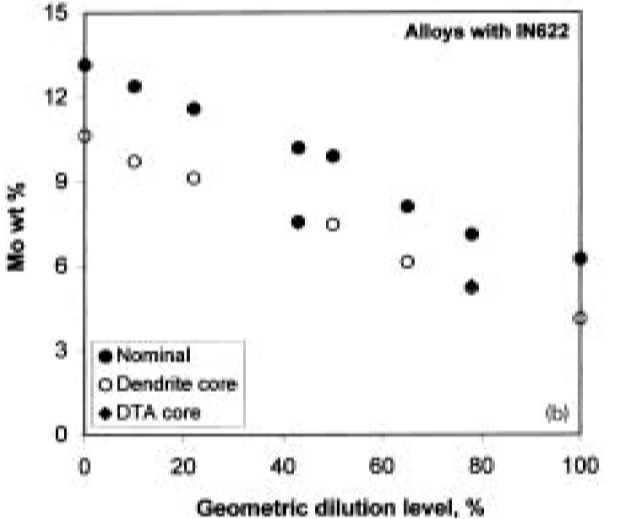
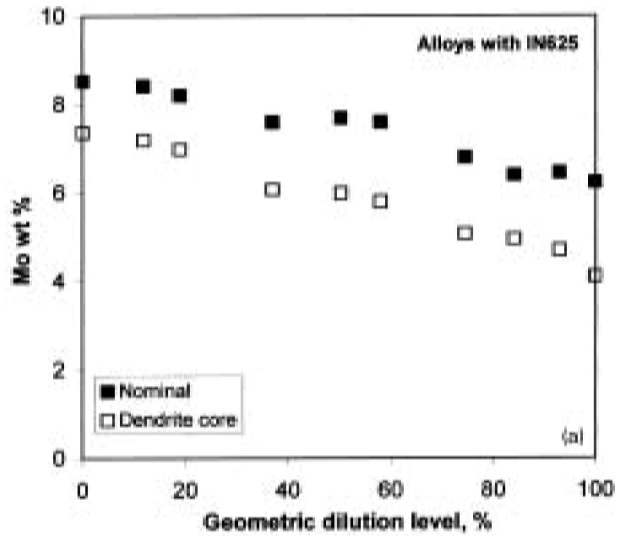
will show little tendency to segregate and the core composition will be close to the nominal composition. The lower the *k* value, the lower the dendrite core concentration of that element.

Table 5 Partition coefficient values for dissimilar metal welds with IN622 filler metal

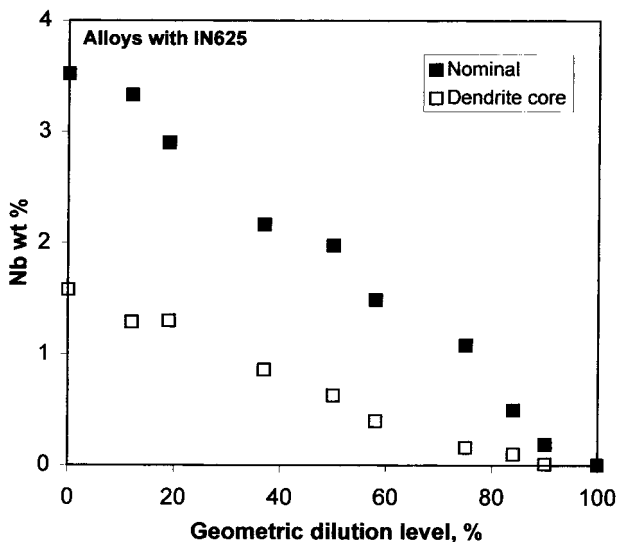
Element	Geometric dilution level							
	100%	78%	65%	50%	43%	22%	10%	0%
Fe	1.06	1.09	1.07	1.17	1.16	1.09	1.04	1.06
Ni	1.02	1.06	1.09	1.03	1.02	1.07	1.07	1.04
Cr	0.99	0.91	0.92	0.91	0.94	0.89	0.93	0.95
Mo	0.65	0.76	0.76	0.75	0.74	0.79	0.79	0.82
Mn	0.76	0.74	0.87	0.87	0.80	0.86	0.84	0.82

Table 6 Partition coefficient values for dissimilar metal welds with IN625 filler metal

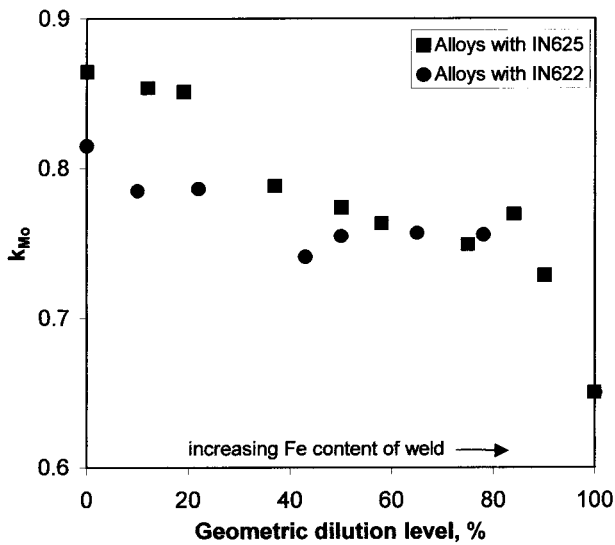
Element	Geometric dilution level								
	90%	84%	75%	58%	50%	37%	19%	12%	0%
Fe	1.09	1.08	1.10	1.12	1.08	1.10	1.09	1.15	1.05
Ni	1.06	1.03	1.04	1.09	1.07	1.06	1.05	1.05	1.03
Cr	0.97	0.91	0.90	0.95	0.84	0.91	0.90	0.93	0.95
Mo	0.73	0.77	0.75	0.76	0.77	0.79	0.85	0.85	0.86
Nb	0.05	0.20	0.15	0.27	0.32	0.40	0.45	0.39	0.45
Mn	0.87	0.89	0.84	0.82	0.83	0.85	0.77	0.83	0.81



13 Nominal and dendrite core Mo concentrations for as welded structures and two differential thermal analysis samples as function of geometric dilution level for a alloys with IN625 and b alloys with IN622



14 Nominal and dendrite core Nb compositions for as welded structures as function of geometric dilution level for alloys with IN625

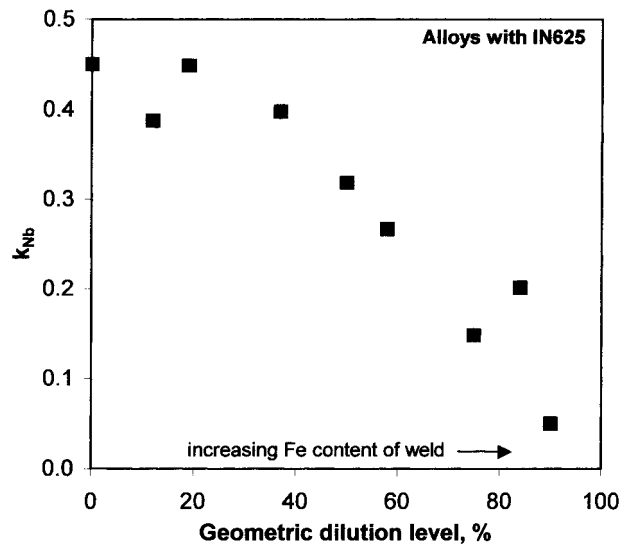


15 Partition coefficient of Mo as function of geometric dilution level for both sets of alloys investigated

It can be seen that all the matrix elements (Fe, Ni, Cr) show little tendency for segregation during solidification (k values close to unity). Since their values are larger than unity, Fe and Ni segregate to the solid, whereas Cr partitions to the liquid. The k values for Mo are relatively low and lie in the range 0.65–0.86. These values are in good agreement with other reported k_{Mo} values in similar alloy systems.¹ As shown in Fig. 15, the Mo partition coefficient decreases as the Fe content in the weld increases (i.e. as the dilution level increases). A similar trend is observed for Nb as shown in Fig. 16. These effects are controlled by the influence of Fe on the solubility of Mo and Nb in austenite and can be explained by consulting the phase diagrams for the Ni–Mo, Fe–Mo, Ni–Nb, and Fe–Nb systems.¹⁶ These diagrams indicate that the maximum solid solubility of Mo in γ -Ni is 35 wt-% (at 1200°C), whereas a maximum of only 2.9 wt-%Mo can be dissolved in γ -Fe (at ~1150°C). A similar trend is observed for Nb, where the maximum solid solubility of Nb in γ -Ni is 18.2 wt-% (at 1286°C), whereas it is only 1.3 wt-% at a similar temperature (1210°C) in γ -Fe. Based upon these observations, Fe additions to Ni base alloys will decrease the solubility of Mo and Nb in austenite. Thus, as the Fe rich dendrites form, the decreased solubility will reduce the amount of Mo and Nb dissolved in the first solid, and increased segregation to the liquid will occur. The general trend of decreasing k values for Mo and Nb with increasing Fe content (Figs. 15 and 16) confirms this. Therefore, the segregation potential of Mo and Nb is a function of the nominal composition of the weld metal. Since the fusion zone composition depends on the arc power and volumetric filler metal feed speed (Fig. 4), the segregation potential of Mo and Nb will be indirectly affected by the welding parameters.

Significance of results

The present results are important from a corrosion perspective. It has been established that the Mo depleted dendrite cores are susceptible to preferential corrosion attack.^{3–6} Overalloying with high Mo filler metals provides a method for increasing the core composition and potentially restoring the corrosion resistance of the weld. Although the nominal weld composition may be high in Mo, the present results show that the dendrite core Mo concentration can be significantly lower than the nominal composition. In addition, the segregation potential is a function of the nominal weld metal composition, which, in turn, is very sensitive to the welding parameters. Therefore,



16 Partition coefficient of Nb as function of geometric dilution level for alloys with IN625

it is recommended that dilution of the high Mo filler metal by the AL–6XN substrate be minimised. Minimising the dilution will have two beneficial effects. First, it will maximise the nominal Mo concentration in the weld, and second, it will restrict the segregation potential of Mo (and Nb). Dilution can be minimised by maximising the volumetric filler metal feedrate to net arc power ratio. However, there exists an area in the fusion zone where complete melting occurs, but mixing between the filler metal and substrate material does not occur. This unmixed zone is located near the fusion line and forms as a result of the presence of a stagnant boundary layer, as shown in Fig. 5. As a result, dendrite core Mo concentrations are expected to be lowest in these areas as the Mo content is not enriched from the filler metal.

SUMMARY

Dilution and microsegregation patterns in dissimilar metal welds between AL–6XN and IN625 and IN622 were investigated. From this work, it has been shown that the dilution level and resultant weld metal composition will depend on the volumetric filler metal feedrate and net arc power. Maximising the ratio of volumetric filler metal feedrate to net arc power will minimise the weld metal dilution level. Additions of Fe to the weld decrease the solubility of Mo and Nb in austenite. As a result, the distribution coefficients of Mo and Nb decrease with increasing Fe content of the weld. This, in turn, produces lower dendrite core concentrations. The Mo core composition is essentially independent of cooling rate over the cooling rate conditions considered in the present work (i.e. those characteristic of arc welding and DTA) owing to the offsetting effects of increased diffusion time and increased length of the concentration gradient that occur with decreasing cooling rate. Minimising the weld metal dilution level will be useful for maintaining corrosion resistance in the weld by maximising the nominal Mo concentration in the weld and minimising the segregation potential of Mo. However, an unmixed zone will always exist near the fusion line that has the same dendrite core composition as that of an autogenous weld in AL–6XN.

ACKNOWLEDGEMENTS

The authors gratefully acknowledge financial support for this work provided by the Office of Naval Research (ONR) under Contract N00014–99–1–0887. Technical discussions

with Dr G. Yoder, ONR throughout the course of the work are also gratefully acknowledged.

REFERENCES

1. J. N. DUPONT: *Weld. J.*, 2000, **78**, 253s–263s.
2. D. PECKNER and I. M. BERSTEIN: 'Handbook of stainless steels'; 1977, New York, McGraw-Hill Book Company.
3. A. TUTHILL and R. AVERY: *Weld. J.*, February 1993, **72**, (2), 41s–49s.
4. T. G. GOOCH: *Weld. J.*, May 1996, **75**, (5), 135s–154s.
5. K. K. BAEK, H. J. SUNG, C. S. IM, I. P. HONG, and D. K. KIM: Proc. Conf. 'Corrosion 98', San Diego, CA, March 1998, National Association of Corrosion Engineers, paper 474.
6. C. D. LUNDIN, W. LIU, G. ZHOU, and C. Y. QIAO: *Weld. Res. Counc. Bull.* January 1998, no. 428.
7. J. I. GOLDSTEIN *et al.*: 'Scanning electron microscopy and X-ray microanalysis', 2nd edn; 1992, New York, Plenum Press.
8. J. N. DUPONT and A. R. MARDER: *Metall. Mater. Trans. B.*, 1996, **27B**, 481–489.
9. S. W. BANOVIC, J. N. DUPONT, and A. R. MARDER: *Weld. J.*, 1999, **78**, (1), 23s–30s.
10. J. F. GRUBB: Proc. Conf. 'Corrosion 96', Denver, CO, March 1996, National Association of Corrosion Engineers, paper 426.
11. M. J. CIESLAK, T. J. HEADLEY, and A. D. ROMIG: *Metall. Mater. Trans. A.*, 1986, **17A**, (11), 2035–2047.
12. M. J. CIESLAK: *Weld. J.*, 1991, **70**, (2), 49s–56s.
13. M. J. CIESLAK, T. J. HEADLEY, G. A. KNOROVSKY, A. D. ROMIG, and T. KOLLIE: *Metall. Mater. Trans. A.*, 1990, **21A**, 479–488.
14. J. N. DUPONT, C. V. ROBINO, and A. R. MARDER: *Acta Mater.*, 1998, **46**, (13), 4781–4790.
15. J. N. DUPONT, C. V. ROBINO, J. R. MICHAEL, M. R. NOTIS, and A. R. MARDER: *Metall. Mater. Trans. A.*, 1998, **29A**, 2785–2796.
16. H. BAKER: 'ASM handbook, vol. 3: alloy phase diagrams'; 1992, Metals Park, OH, ASM International.